FULL PAPER

Ttriboelectric Nanogenerators

ADVANCED
FUNCTIONAL
MATERIALS

www.afm-journal.de

High Energy Storage Efficiency Triboelectric Nanogenerators with Unidirectional Switches and Passive Power Management Circuits

Huaifang Qin, Gang Cheng,* Yunlong Zi,* Guangqin Gu, Bao Zhang, Wanyu Shang, Feng Yang, Junjie Yang, Zuliang Du, and Zhong Lin Wang*

The high-voltage and low-current output characteristics of a triboelectric nanogenerator (TENG) make itself difficult for directly powering small electronic devices. A power management circuit (PMC) is indispensable to address the impedance mismatch issue. In this paper, a TENG with a unidirectional switch (TENG-UDS) is developed, which can provide the maximized output energy regardless of the load resistance. A passive PMC with a simple structure and high energy storage efficiency is designed based on this TENG-UDS, which is made up of all passive electronic components, including an inductor, a diode, and a capacitor. Theoretical calculations show that the theoretical energy storage efficiency of the passive PMC can reach 75.8%. In the actual experiment of charging a capacitor, the measured energy storage efficiency can reach 48.0%. It is demonstrated that the electronic watch and high-brightness quantum dot light-emitting diode can be driven by using the TENG-UDS with the passive PMC, which cannot be achieved without the PMC. The passive PMC for TENG-UDS has the advantages of simple structure, low energy consumption, and high energy storage efficiency, which provides a promising method for the power management and practical application of TENG.

1. Introduction

The internet of things (IoT) aims at realizing the interconnection between objects through sensing, processing, and transmission of the information. The sensing terminal is a key part in the IoT, which converts various parameters in physical world, such as temperature, humidity, light intensity, pressure, and so on, into digital signals. In the IoT, the sensors consume a very little amount of energy, but they are huge in number and widely distributed with possibility of mobile. If they are driven by using batteries, it will not only lead to difficulties in battery's tracking and recovery, but also cause environmental pollution and health hazards. Therefore, it is urgently needed to develop novel energy technology that can continuously supply power to small electronic devices. Recently, triboelectric nanogenerator (TENG) has been invented through coupling the triboelectrification and electrostatic induction effects, which can directly convert mechanical energy from the environment and human motion into electricity.[1–4] Based on various working modes of TENG,[5–15] many self-powered sensors have been developed, which can be used to detect temperature,[16] light,[17] gas,[18] sound,[19] sphygmus,[20] and so on.

TENG has the characteristics of high voltage and low current, which is not suitable for directly driving small electronic devices. Therefore, power management circuit (PMC) is necessary to efficiently store the energy generated by TENG in a battery or a capacitor. TENG has high output impedance, generally in the range from 1 to 10 MΩ.[21–23] However, the input impedance of common PMCs is only several kΩ. For developing PMCs with high energy storage efficiency, the impedance mismatching problem

H. F. Qin, Prof. G. Cheng, Dr. G. Q. Gu, Dr. B. Zhang, W. Y. Shang,
F. Yang, J. J. Yang, Prof. Z. L. Du
Key Lab for Special Functional Materials
Ministry of Education
National and Local Joint Engineering Research Center
for High-Efficiency Display and Lighting Technology
School of Materials Science and Engineering
and Collaborative Innovation Center of Nano Functional Materials
and Applications
Henan University
Kaifeng 475004, China
E-mail: chenggang@henu.edu.cn

Prof. G. Cheng, Prof. Y. L. Zi, Prof. Z. L. Wang
School of Materials Science and Engineering
Georgia Institute of Technology
Atlanta, GA 30318, USA
E-mail: ylzi@cuhk.edu.hk; zlwang@gatech.edu

Prof. Y. L. Zi
Department of Mechanical and Automation Engineering
The Chinese University of Hong Kong
Shatin, N.T., Hong Kong SAR, China

Prof. Z. L. Wang
Beijing Institute of Nanoenergy and Nanosystems
Chinese Academy of Sciences
Beijing 100083, China

**ADVANCED
SCIENCE NEWS**
www.advancedsciencenews.com

**ADVANCED
FUNCTIONAL
MATERIALS**
www.afm-journal.de

is necessary to be solved. In our previous report, a mechanical trigger switch has been introduced to modulate the output performances of TENG.[24–30] Through this method, we can obtain constant output voltage and maximized output energy regardless of the load resistance.[24] The theoretical calculations also show that the utilization of a switch is the key for solving TENG's impedance mismatching problem and achieving the maximum output energy.[28] Due to the excellent impedance matching characteristics, the switch has been used for developing high energy storage efficiency PMCs for TENG. Several groups have already used metal oxide semiconductor field effect transistor (MOS-FET) and other electronic components as switches to develop TENG's PMC,[22,31,32] and the maximum energy storage efficiency of 60% has been obtained.[22] However, the switches in these PMCs are composed of active electronic components, such as MOS-FET, and additional power is needed to drive the switches. The active electronic components increase the complexity and manufacturing cost of the PMC system, and produce additional energy loss. Therefore, in order to develop PMCs with high energy storage efficiency and low cost, it is of great significance to designing passive PMC on the basis of passive switch.

In this paper, a TENG with a unidirectional switch (TENG-UDS) was developed, which can provide maximized output energy regardless of the load resistance. Based on this TENG-UDS, a passive PMC was designed, which was composed of all passive electronic components, including an inductor, a diode, and a capacitor. This passive PMC has the advantages of simple structure, low energy consumption, and high energy storage efficiency. No additional power source is needed in the passive PMC. And the unidirectional switch decreases the number of diodes used in the PMC and reduces the energy loss induced by the diodes. The theoretical calculations and simulations showed that the maximum energy storage efficiency can reach 75.8%. In the actual experiment, the energy storage efficiency reached 48.0%. It was demonstrated that the electronic watch and high-brightness quantum dot light-emitting diode (QLED) can be driven by using the passive PMC.

2. Results and Discussion

2.1. The Design and Working Mechanism of the TENG-UDS

The structure diagram of the TENG-UDS is shown in **Figure 1**a. Here, we use the freestanding triboelectric-layer mode of TENG to demonstrate the structure and working mechanism of the unidirectional switch. The triboelectric layer and electrode layer of the TENG are composed of polytetrafluoroethylene (PTFE) film and Cu electrode, respectively. The unidirectional switch
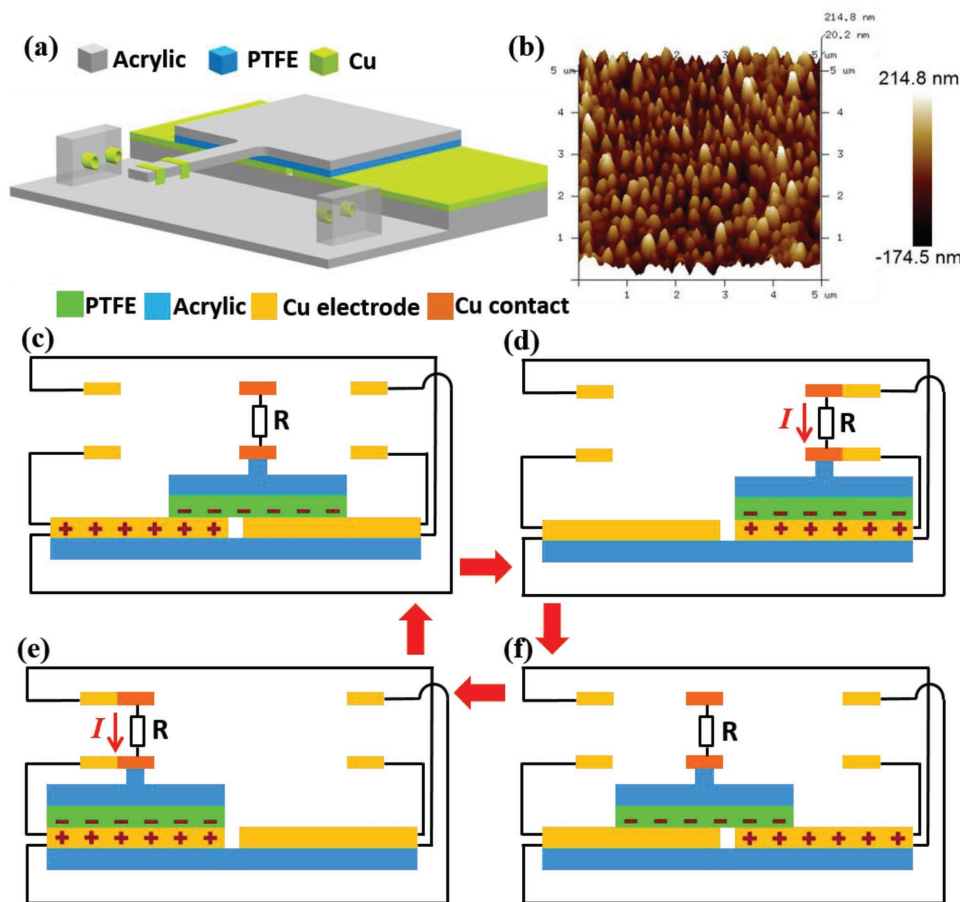

Figure 1. a) The structure diagram of the TENG-UDS. b) The AFM image of the RIE etched PTFE film. c–f) The working mechanism diagram of the TENG-UDS.

**ADVANCED
SCIENCE NEWS**
www.advancedsciencenews.com

**ADVANCED
FUNCTIONAL
MATERIALS**
www.afm-journal.de

consists of two moving contacts and four stationary spring contacts. Two moving contacts are fixed on the acrylic cantilever of the triboelectric layer and move along with the triboelectric layer. Two stationary spring contacts are placed on the outside of each Cu electrode layer. The surface of the PTFE film is modified by the reactive ion etching (RIE) process, and the atomic force microscope (AFM) image of the etched PTFE film are shown in Figure 1b. After etching, the nanoscale convex and concave structure were produced to increase the roughness on the PTFE surface, which can improve the effective contact area of the triboelectric layer and further enhance the output performance of the TENG.[33,34]

The working mechanism of the TENG with a switch has been discussed in detail in our previous reports.[24–30] Briefly, as shown in Figure 1c–f, when the PTFE layer moves to the right-hand side (Figure 1d) and left-hand side (Figure 1e), respectively, the switch is closed, and a pulsed output is generated. With the switch, the transferred charge reaches the maximum value,

Q_{max}, and the output voltage can be accumulated to the maximum value, $\pm V_{max}$, regardless of load resistance. With previous switches,[24–30,35] there are two electrical output with opposite direction in a moving cycle of TENG. However, as the unidirectional switch is used here, the two electrical output in a cycle would have same direction. This is because that the connections between the two moving contacts and the two Cu electrodes are changed in the two half cycles. In the half cycle of right sliding and left sliding, the upper moving contact is connected with left and right Cu electrode, respectively, as shown in Figure 1d,e.

2.2. The Output Characteristics of the TENG-UDS

Figure 2a shows the output current curve of the TENG-UDS, where the load resistance is 20 MΩ and the motion frequency of the TENG is 1 Hz. The unidirectional pulsed current peaks are obtained with a peak height of ≈17.5 µA, and
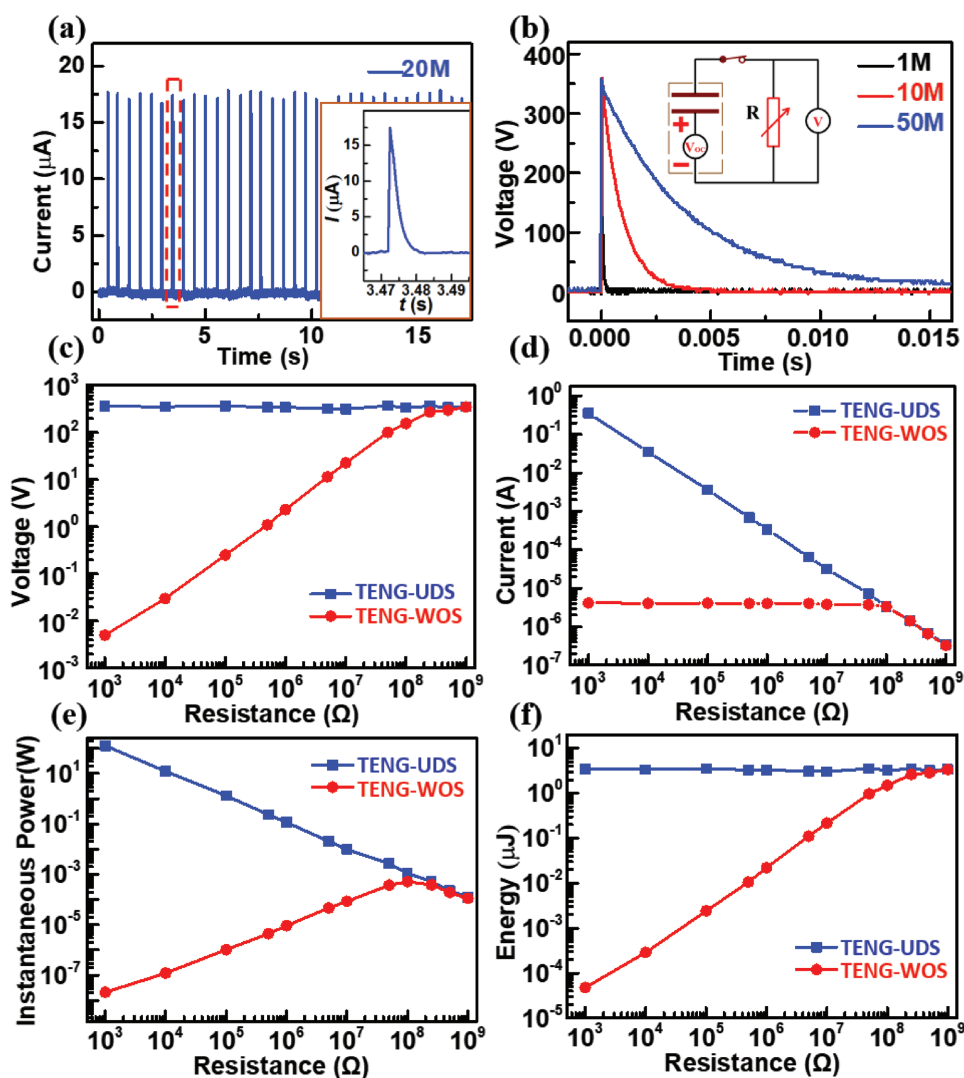

Figure 2. a) Output current curve of the TENG-UDS with a load of 20 MΩ, and the enlarged view is shown in the inset. b) Output voltage curves of the TENG-UDS with loads of 1, 10, and 50 MΩ, respectively. Inset is the circuit diagram of measuring the output voltage of the TENG-UDS. The dependences of c) voltage peak, d) current peak, e) power peak, and f) output energy on resistance for TENG-UDS and TENG-WOS, respectively.

**ADVANCED
SCIENCE NEWS**

www.advancedsciencenews.com

**ADVANCED
FUNCTIONAL
MATERIALS**

www.afm-journal.de

the frequency of the current peaks is 2 Hz. This verifies that the unidirectional output is obtained. As shown in the inset of Figure 2a, the current increases suddenly from zero to the peak, and then slowly drops to zero. The position of the pulsed peak corresponds to the moment the switch is closed. Figure 2b shows the output voltage curves for external loads of 1, 10, and 50 MΩ, respectively. The inset is the circuit diagram of measuring the output voltage of the TENG-UDS. It is found that the peak values remain almost same about 350 V. However, the peak width is gradually widened with the increase of resistance. For the pulsed mode TENG with a switch, the output voltage's change over time satisfies the equation[24]

$$V = V_{max}e^{-t/\tau} \tag{1}$$

Here, τ is the decay time constant of the voltage and equals to RC, where R is the load resistance and C is the TENG's equivalent capacitance. See ref. [24] for detailed derivation of Equation (1). According to Equation (1), τ is proportional to its load resistance. The calculated τ at loads of 1, 10, and 50 MΩ are 0.61×10^{-4}, 0.88×10^{-3}, and 0.39×10^{-2} s, respectively, which are nearly proportional to the load resistance.

The dependences of instantaneous voltage peak (V_p), instantaneous current peak (I_p), instantaneous power peak (W_p), and output energy in a half cycle (E) on load resistances ranging from 1 kΩ to 1 GΩ are shown in Figure 2c–f. For a freestanding triboelectric-layer mode of TENG, the theoretical maximized E in half cycle satisfies the equation[36]

$$E_{max} = \frac{1}{2}Q_{max}V_{max} \tag{2}$$

The derivation of Equation (2) is shown as Equations (S1)–(S4) (Supporting Information). In the actual test process, the output energy is calculated by integrating current under different loads according to Equation (3)

$$E = \int I^2 R \, dt \tag{3}$$

As a comparison, the electrical output of the conventional TENG without a switch (TENG-WOS) are also plotted here. For TENG-UDS, V_p and E are regardless of R, which are constant about 350 V and 3.33 µJ in the range from 1 kΩ to 1 GΩ. Figure S2 (Supporting Information) shows the output voltage under the load resistance of 1 kΩ. I_p and W_p are proportional to $1/R$. As R is reduced from 1 GΩ to 1 kΩ, I_p and W_p increase from 3.54×10^{-7} A and 1.25×10^{-4} W to 0.36 A and 126.74 W, respectively. It is worth noting that the obtained peak value of 126.74 W is the instantaneous power peak of the TENG-UDS under a load resistance of 1 kΩ. By considering the narrow peak width less than 1 µs and the time interval of 0.5 s between two peaks, it is calculated that the average power is only 6.67 µW. For TENG-WOS, V_p and E are almost linear with R, which are only 5 mV and 4.81×10^{-5} µJ, respectively, as R is 1 kΩ. The measured electrical output characteristics of the TENG-UDS are in good accordance with the theoretical calculation results of the TENG with a switch, where the output voltage peak is equal to the open-circuit voltage and E is maximized, regardless of R.[24,36] In addition, the output voltage of TENG-UDS

remains unchanged at 1 kΩ. As we know, if the internal load resistance is larger than the external resistance of the TENG, the output voltage will decrease, so the internal resistance of TENG-UDS should be lower than 1 kΩ.

In addition, the effect of sliding speed and the force exerted on the triboelectric layer was investigated. by connecting a 50 MΩ resistor in series with the TENG-UDS. The sliding speeds were set to be 0.06, 0.17, and 0.51 m s^{-1}, respectively. As shown in Figure S1 (Supporting Information), the currents are almost the same and the peak value is about 7 µA, and the feature is of great significance when collecting irregular mechanical energy in the environment. Pressures of 1.0, 3.2, 4.2, 5.3, 6.5, and 7.4 N were applied to the triboelectric layer, respectively. The output current increases from about 6.5 to 8.5 µA. Considering that the TENG-UDS will be used to collect mechanical energy in the environment in the future and to maintain a smooth motion, we set the applied pressure in the range of 1–3 N in the experiment.

2.3. The Passive PMC Based on TENG-UDS

Based on the excellent impedance matching and unidirectional output characteristics of TENG-UDS, a passive PMC is designed, which is composed of three simple passive components including one inductor, one diode, and one capacitor. The schematic diagram of its structure and working principle is shown in **Figure 3**a,b. In this passive PMC, TENG-UDS is equivalent to the series connection of a voltage source (V_{OC}) and a capacitor C_1. There are two parallel circuits connected to the output of the TENG-UDS. One circuit consists of an inductor L, and the other circuit consists of a storage capacitor C_2 and a diode D_1 in series. Through the passive PMC, the electrical energy output of TENG-UDS is stored in C_2. The energy storage process is divided into the following two stages. In the first stage (Figure 3a), the electrical energy of TENG-UDS is converted into magnetic energy and stored in L. In the second stage (Figure 3b), the magnetic energy of L is converted into electrical energy and stored in C_2.

As the switch is closed, the first energy transfer stage begins. Since TENG-UDS has a positive output voltage, D_1 is reversely biased and turned off. Therefore, the branch of C_2 is open. As a result, the TENG-UDS only forms an electrical loop with L and generates a current on L (I_L). With the increase of I_L, the magnetic energy stored in L increases gradually. When I_L reaches the maximum, the electrical energy of TENG-UDS is completely transformed into magnetic energy and stored in L. Subsequently, I_L gradually decreases, and a negative self-inductance voltage is generated by L, which is applied to the branch of D_1 and make D_1 forward biased. As D_1 is turned on, an electrical loop between L and C_2 is formed, and then the second energy transfer stage begins. In this stage, the magnetic energy of L is converted into electrical energy and stored on C_2. After the energy storage is completed, D_1 is reversely biased and turned off again, and then C_2 is disconnected with L, which allows the stored electrical energy to be remained on C_2. Now, one charging cycle is completed. In one motion cycle of the TENG-UDS, the switch is closed twice, and two charging cycles occur.
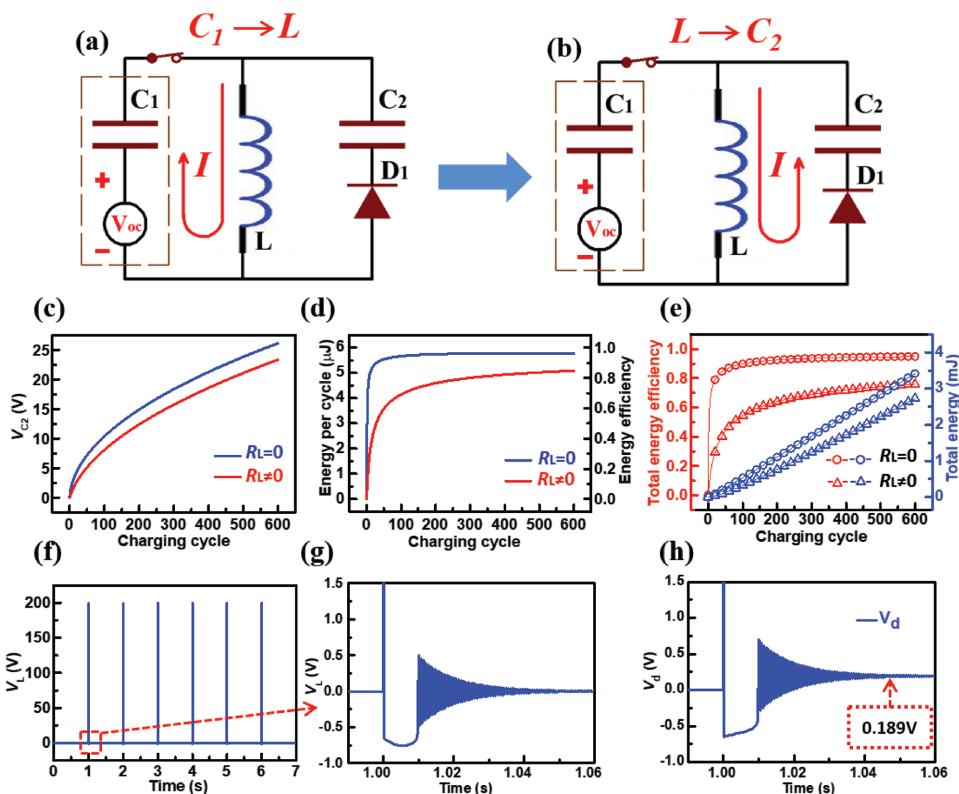
Figure 3. a,b) The working mechanism of the passive PMC for TENG-UDS in the first and second energy transfer stages. c) Dependences of calculated voltage of the capacitor C_2, d) stored energy and its energy storage efficiency of each charging cycle, and e) totally stored energy and its energy storage efficiency on charging cycles, with an ideal and an actual inductor, respectively. f) The simulated curve of V_L during multiple charging cycles, and g) the enlargement for the first charging cycle. h) The simulated curve of V_d for the first charging cycle.

2.4. The Equations Expression of the Charging Cycles of the PMC

In order to understand more deeply about the charging cycle and the source of energy loss in this passive PMC, a theoretical calculation has been performed. First, we calculate the charging cycle with an ideal inductor, where the series resistance of L, R_L, is zero. Here, the current of L is defined as I_L, and the voltage across L, V_L, and magnetic energy of L, E_L, are expressed as

$$V_L = L\frac{dI_L}{dt} \tag{4}$$

$$E_L = \frac{1}{2}LI_L^2 \tag{5}$$

In the first energy transfer stage as shown in Figure 3a, D_1 is turned off and the TENG-UDS is in parallel with L. Therefore, V_L is equal to the voltage across the TENG-UDS, which is described as

$$L\frac{d^2Q}{dt^2} = V_{OC} - \frac{Q_1}{C_1} \tag{6}$$

where Q is the transferred charge from TENG-UDS to L, V_{OC} is the open-circuit voltage of the TENG-UDS, and Q_1 is the charge

on C_1. At the moment as the switch is closed ($t = 0$), $Q_1 = 0$. The expression of V_L can be obtained as

$$V_L = V_{OC}\cos(\omega_1 t) \tag{7}$$

where $\omega_1 = 1/\sqrt{LC_1}$. According to Equations (4)–(7), when I_L reaches the maximum, V_L equals zero and E_L reaches the maximum. In the second energy transfer stage as shown in Figure 3b, the expression of V_L is described by

$$L\frac{d^2Q}{dt^2} = V_{OC} - \frac{Q_1}{C_1} = V_{th} - \frac{Q_2}{C_2} \tag{8}$$

where Q_2 is the charge of C_2, $V_{th} = -(V_D + V_{C2})$, V_D is turn-on voltage of D_1, and V_{C2} is the initial voltage of C_2. Here, V_{th} represents a threshold voltage of V_L, where D_1 is turned on and the second energy transfer stage begins. Here, $Q = Q_1 + Q_2$. Finally, V_L is expressed as

$$V_L = V_{th}\cos(\omega_2 t) - \frac{C_1}{C_1 + C_2}\frac{\omega_1}{\omega_2}\sqrt{V_{OC}^2 - V_{th}^2}\sin(\omega_2 t) \tag{9}$$

where $\omega_2 = 1/\sqrt{L(C_1 + C_2)}$. According to Equation (9), the absolute value of V_L increases first and then drops. As it drops to V_{th}, D_1 is turned off and the second energy transfer stage is completed. During one charging cycle, the voltage of C_2 is increased from V_{C2} to

**ADVANCED
SCIENCE NEWS**
www.advancedsciencenews.com

**ADVANCED
FUNCTIONAL
MATERIALS**
www.afm-journal.de

$$\sqrt{\frac{C_1}{C_1 + C_2} V_{OC}^2 + \frac{C_2}{C_1 + C_2} V_{th}^2} - V_D \qquad (10)$$

After that, the remained magnetic energy in L will oscillate between L and C_1. The equivalent circuit of this process is the same as the first energy transfer stage, which is also described by Equations (6) and (7). However, since C_1 is much less than C_2, this part of energy consumption can be approximately ignored. For the passive PMC with an actual inductor, where R_L is not zero, the expressions of the charging cycles can also be obtained, which are shown as Equations (S5)–(S9) (Supporting Information).

By solving Equation (10) and Equation (S9) (Supporting Information), the values of V_{C2} during 600 charging cycles are calculated and plotted in Figure 3c, where the parameters of the electrical components in the PMC are listed in Table S1 (Supporting Information). After 600 charging cycles, V_{C2} with ideal inductor ($R_L = 0$) and actual inductor ($R_L = 7.2$ kΩ) are increased to 26.14 and 23.37 V, respectively. The stored energy in C_2 for each charging cycle and its corresponding energy storage efficiency are shown in Figure 3d, where C_2 is 10 μF. Here, the energy storage efficiency is defined as the ratio of the added energy in C_2 and the output energy of the TENG-UDS in a single charging cycle. For ideal inductor, the stored energy increases rapidly in the first 50 charging cycles, and then reaches saturation. In the 600th charging cycle, the energy storage efficiency reaches 96.1%. For actual inductor, the stored energy increases rapidly in the first 100 cycles, and then increases slowly. In the 600th charging cycle, the energy storage efficiency reaches 84.8%.

The total energy stored in C_2 and its corresponding energy storage efficiency during the 600 charging cycles are shown in Figure 3e. For the ideal inductor, the total energy storage efficiency increases rapidly in the first 100 cycles, and then reaches saturation. The total energy storage efficiency values after 10, 50, 100, 200, and 600 charging cycles are 71.7, 86.1, 89.8, 92.5, and 94.9%, respectively. For the actual inductor, the total energy storage efficiency increases rapidly in the first 200 cycles, and then increases slowly. The total energy storage efficiency values after 10, 50, 100, 200, and 600 charging cycles are 19.7, 43.5, 54.5, 63.9, and 75.8%, respectively. For the PMC with an ideal inductor, the energy loss comes from two aspects: one is the generated potential across the diode, the other is the LC oscillation between L and C_1. When the ideal inductor is replaced by the actual inductor with series resistance, the total energy storage efficiency after 600 charging cycles is reduced from 94.9 to 75.8%, which indicates that the series resistance of L is a major factor for energy loss in the PMC.

2.5. The Circuit Simulations of the Passive PMC

In order to verify the theoretical calculation results, the circuit simulation method is used to simulate the passive PMC designed for TENG-UDS. In the simulation, an actual inductor with a series resistance was used, and the parameters of the electronic components are the same as those used in the theoretical

calculation. The simulated results are shown in Figure S3 (Supporting Information), which are similar to the theoretically calculated results shown in Figure 3c–e. Also, the simulated values are almost same with those obtained by theoretical calculation. As a quantitative comparison for the totally energy storage efficiency after 600 charging cycles, the simulated value of 74.7% is only slight less than the theoretically calculated value of 75.8%. In the theoretical calculation, the diode is simplified as an ideal diode with a turn-on voltage of 0.58 V. However, in the simulation, the current–voltage characteristic of the diode is considered, which is considered as the reason for the slight increase of energy loss in the PMC.

Figure 3f shows the simulated curve of the voltage on inductor, V_L, during multiple charging cycles, and the enlarged view of the first charging cycle is shown in Figure 3g. As the switch is closed, V_L instantaneously increases from 0 to a maximum of 200 V, and then sharply drops and becomes negative, which corresponds to the first energy transfer stage. As V_L reaches −0.65 V, the diode is turned on, and the second energy transfer stage begins. During the following 10 ms, the absolute value of V_L first increases and then decreases, which is in accordance with the expression of V_L by Equation (9). When the absolute value of V_L is less than 0.51 V, the damping oscillation is generated between L and C_1, which indicates that the diode is turned off and the energy storage is completed. Different with the theoretical calculation results, the simulated threshold voltage values for turning on (0.65 V) and turning off (0.51 V) the diode are not exactly same as the turn-on voltage of the diode (0.58 V), which is attributed to the current–voltage characteristic of an actual diode. The simulated curve of the voltage on diode, V_d, for the first charging cycle is shown in Figure 3h, and the curve for multiple charging cycles is shown in Figure S4 (Supporting Information). The curve of V_d is similar to that of V_L. However, as the damping oscillation between L and C_1 is completed, V_d does not decay to zero but remains at 0.189 V, which represents the voltage of C_2 after the first charging cycle.

2.6. The Measured Properties of the Passive PMC

Next, the practical performances of the passive PMC for TENG-UDS are measured. The same TENG-UDS device measured in Figure 2 is used here, which has an open-circuit voltage about 350 V. The turn-on voltage and the reverse breakdown voltage of the diode (FRED, HER 208) are 1.7 and 1000 V, respectively. **Figure 4**a shows the measured current of L, I_L, in a charging cycle, and the inset shows the enlargement. We can see that I_L rapidly increases from zero to the peak about 198 μA in 0.6 ms, and then slowly declines to zero in 47 ms. The rising and falling periods correspond to the first and second energy transfer stages, respectively. Based on Equation (4), V_L is calculated by using the measured I_L curve, and the curve of V_L and its enlargement are shown in Figure 4b,c, respectively. These curves are in good accordance with the simulated V_L curves in Figure 3f,g, which confirm the working mechanism of the passive PMC discussed above. The magnetic energy in L, E_L, is calculated by Equation (5) and shown in Figure 4d. The peak of E_L is 3.14 μJ, which reaches as high as 94.3% of the output
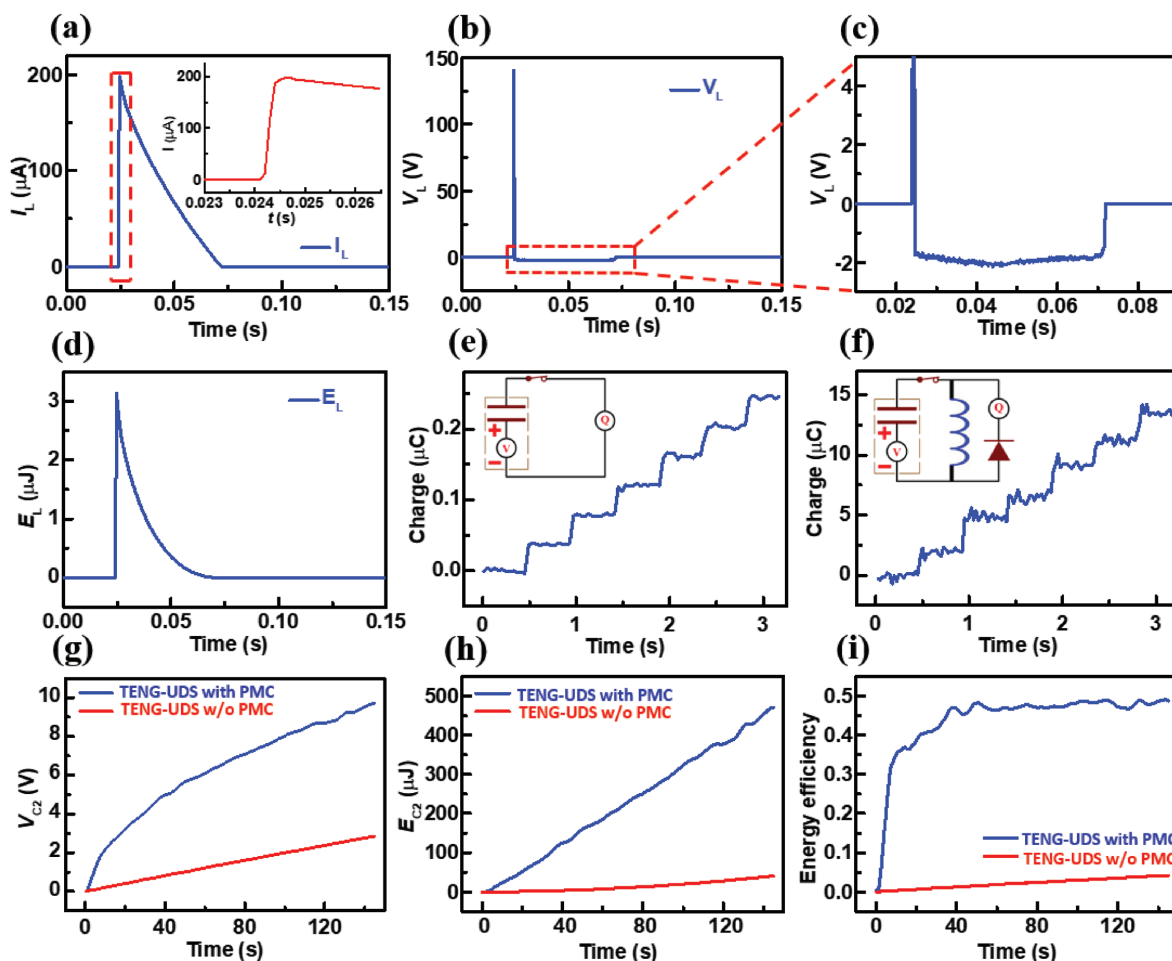
Figure 4. a) The measured curve of the I_L in a charging cycle, and the inset shows the enlargement. b,c) The curve of V_L in a charging cycle and its enlargement. d) The curve of the energy of L in a charging cycle. e,f) The collected charge of TENG-UDS in six charging cycles without and with PMC, respectively, and the insets show the circuit diagrams. g) The measured voltage of C_2, h) the totally stored energy in C_2, and i) the total energy storage efficiency of the TENG-UDS with and without PMC, respectively.

energy of the TENG-UDS about 3.33 μJ. This means that the energy loss in the first energy transfer stage is about 5.7%. The transferred charge of the TENG-UDS without and with the passive PMC are measured, which are shown in Figure 4e,f, respectively. With the PMC, the collected charge in six charging cycles reaches 13.5 μC, which is 56 times higher than that without the PMC (0.24 μC).

The voltage of C_2, V_{C2}, during the charging cycles is measured and plotted in Figure 4g, where C_2 is 10 μF, the motion frequency of the TENG-UDS is 1 Hz, and the average output energy of the TENG-UDS in 1 s is 6.66 μJ. As a control experiment, V_{C2} as charged by the same TENG-UDS without the PMC is also measured. The totally stored energy in C_2 and the energy storage efficiency are calculated and plotted in Figure 4h,i, respectively. In the case without using the PMC, V_{C2} increases linearly with time, the stored energy increases in a power law with a power exponent of 2, and the energy storage efficiency increase almost linearly. After 145 s (290 charging cycles), V_{C2}, the stored energy and the energy storage efficiency reach 2.84 V, 40.36 μJ, and 4.2%, respectively. With the passive PMC, V_{C2} increases in a power law with a power exponent of

0.5, which reaches 9.70 V after 145 s. In the first 5 s, the stored energy increases in a power law with a power exponent of 2, and then increase almost linearly in the following charging cycles. After 145 s, the stored energy reaches 470.73 μJ, which has a nearly 12-fold improvement over that without using the PMC. The total energy storage efficiency rapidly increases to 40.8% in the first 10 s, and then increases slowly and reaches saturation after 40 s. The maximum energy storage efficiency reaches as high as 48.0%.

By using the passive PMC, the electrical energy of TENG-UDS with high voltage can be efficiently stored on a capacitor, which can be used as a power supply for small electronic devices. **Figure 5**a shows the circuit diagram of driving electronic devices by using the passive PMC, where the electronic devices are parallel to C_2. First, it is demonstrated to drive an electronic watch. As shown in Figure 5b, after three charging cycles about 1.5 s, the electronic watch starts to work normally and last for 4 s (Video S1, Supporting Information). As the TENG-UDS operates continuously at a frequency of 1 Hz, the electronic watch can work continuously. Next, it is demonstrated to drive a QLED with high output power
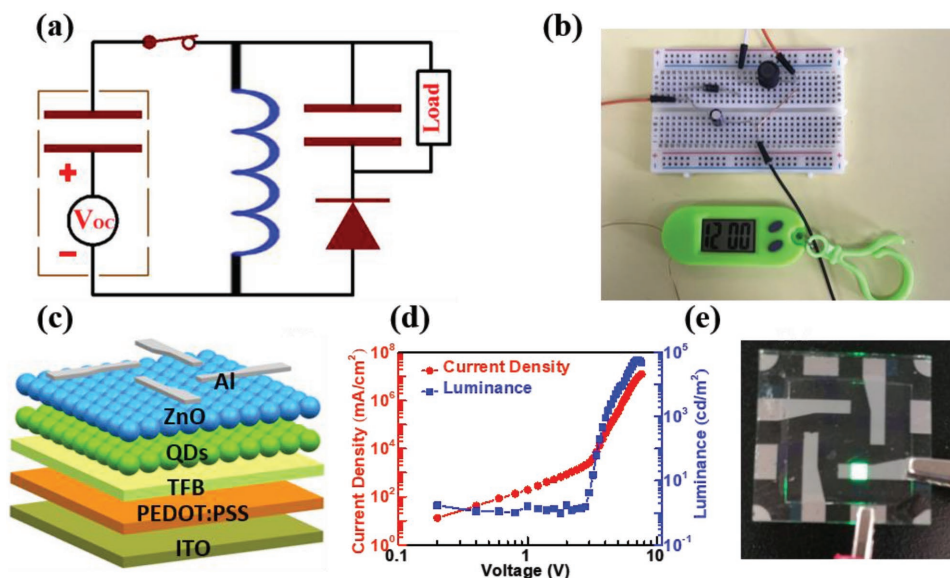
Figure 5. a) The circuit diagram of the TENG-UDS with the passive PMC for driving electronic device. b) The picture of the normal work of a commercial electronic watch driven by the PMC. c) The structure diagram of the QLED. d) Dependences of current density and luminance on voltage for the QLED. e) The picture of the lighted QLED driven by the PMC.

and driving current by using the passive PMC with a C_2 of 100 µF. A switch is installed between C_2 and the QLED. As C_2 is charged to a certain voltage, the switch is closed. The structure diagram of the QLED is shown in Figure 5c, and the dependences of its luminescence intensity and current density on voltage are shown in Figure 5d. The luminescence intensity suddenly rises when the voltage reaches 2.5 V, and the QLED starts to emit light. The breakover point of current curve is a little lagged behind the luminance curve, which may be caused by the sub-bandgap electroluminescence from QLED and Auger-assisted energy upconversion process.[37–39] For device with a size of 4 mm², the output power and driving current at 3 V are 0.78 mW and 0.26 mA, respectively. After 140 charging cycles about 70 s, C_1 is charged to 3.02 V, which can drive the QLED with bright light for 3 s, as shown in Figure 5e. For a comparison, 1100 charging cycles about 550 s is needed to drive the QLED, as the TENG-UDS operates without the PMC. And we have tried to drive the QLED using the conventional sliding TENG and the passive PMC. However, due to TENG-UDS has a huge mismatch with the impedance of the inductor in PMC, the energy of TENG-UDS cannot be transferred into the PMC, the voltage of the capacitor is still 0 V after 1500 cycles.

As discussed above, the passive PMC can effectively improve the energy storage efficiency of the TENG-UDS, which has promising applications in driving electronic devices. The high energy storage efficiency of the passive PMC comes from three aspects. First, the output voltage and energy of the TENG-UDS are maximized and regardless of the load resistance, which has excellent impedance matching with the PMC. Second, no active electronic components are used in the PMC, which simplifies the circuit and reduces the energy loss. Last but not least, the unidirectional electrical output is obtained in the TENG-UDS, which decreases the number of diodes used in the PMC and reduces the energy loss induced by the diodes.

However, the maximum energy storage efficiency of 48.0% in the real measurement is less than the theoretically calculated value of 75.8%. As discussed in Figure 4d, the efficiency of the energy stored in L in the first energy transfer stage can reach as high as 94.3%. This means the most energy loss occurs in the second energy transfer stage. During this stage, it is considered that the diode is a major source for the energy loss. As shown in Table S2 (Supporting Information), it is found that if the diodes with longer reverse recovery time and lower reverse breakdown voltage are used in the PMC, the collected charge in a charging cycle is reduced from 2.45 to 0.50 µC. The energy loss caused by the diode mainly comes from two aspects. First, the equivalent capacitance of the diode will store a part of energy. Second, during the diode's recovery time from turn-on state to turn-off state, large reverse leakage current is driven by the voltage of C_2, which causes the leakage of the charges and energy stored in C_2. The energy storage efficiency of the PMC can be further improved by optimizing the parameters of the diode and other components in our investigations in the future.

3. Conclusion

In this paper, a TENG with a unidirectional switch, TENG-UDS, has been developed, in which its electrical output is unidirectional. The TENG-UDS can provide maximized output voltage and output energy regardless of the load resistance, which has excellent impedance mismatch with the PMC. Based on the TENG-UDS, a passive PMC with simple structure and high energy storage efficiency was designed, which was made up of all passive electronic components, including an inductor, a diode, and a capacitor. Theoretical calculations showed that the theoretical energy storage efficiency of the passive PMC can reach 75.8%. In the actual

experiment, the measured energy storage efficiency can reach 48.0%. It was demonstrated that the electronic watch and the QLED with high output power and driving current can be driven by using the passive PMC. The passive PMC based on the TENG-UDS has the advantages of simple structure, low energy consumption, and high energy storage efficiency, which provides promising method for the power management and practical application of TENG.

4. Experimental Section

The Design of the TENG-UDS: First, the freestanding triboelectric-layer mode was used to design the TENG-UDS. A laser cutting machine was used to fabricate a certain shape of acrylic plate as a supporting material, and two copper tapes with lengths, widths, and thicknesses of 80 mm, 80 mm, and 0.05 mm were attached as left and right electrodes, and the distance between the two electrodes is 2 mm. Then a PTFE film with a thickness of 0.1 mm was adhered to the other acrylic plate as a triboelectric layer. The unidirectional switch consists of two moving contacts and four stationary spring contacts. Two moving contacts were fixed on the cantilever of the triboelectric layer and move along with the triboelectric layer. Two stationary spring contacts were placed on the outside of each Cu electrode layer and connected to two Cu electrodes, and the two moving contacts were connected to the external load and the test meter. The length and the outer diameter of the spring in the stationary spring contact are both 5 mm. The moving contact is two U-shaped copper spring plates. The thickness and width of the spring plate are 0.5 mm and 5 mm, respectively. The two spring pieces are not in contact with each other and placed in parallel, and the spacing of the spring pieces is consistent with the spacing of the two spring contacts on one side. Finally, the surface of the PTFE film was etched by the reactive ion beam as follows. The chamber pressure was set to 200 mTorr, the power was 100 W, the flow rates of O_2, Ar, and CF_4 were 10.0, 15.0, and 30.0 sccm, respectively. And the etching time was 6 min.

The Measurement of Electrical Signals of the TENG-UDS: The measurements were carried out at room temperature and air atmosphere. The output current of the TENG-UDS was measured using a low-noise current preamplifier (Model SR570, Stanford Research System). The multifunctional electrometer (Model 6514, Keithley) was used to test the transfer charge of the TENG-UDS and the charging voltage of the capacitor. In addition, the oscilloscope (Model TBS 1104, Tektronix) was used to measure the output voltage of the TENG-UDS.

Supporting Information

Supporting Information is available from the Wiley Online Library or from the author.

Conflict of Interest

The authors declare no conflict of interest.

[1] F. R. Fan, Z. Q. Tian, Z. L. Wang, *Nano Energy* **2012**, *1*, 328.
[2] Z. L. Wang, J. Chen, L. Lin, *Energy Environ. Sci.* **2015**, *8*, 2250.
[3] Y. L. Zi, H. Y. Guo, Z. Wen, M. H. Yeh, C. G. Hu, Z. L. Wang, *ACS Nano* **2016**, *10*, 4797.
[4] C. Zhang, W. Tang, C. B. Han, F. R. Fan, Z. L. Wang, *Adv. Mater.* **2014**, *26*, 3580.
[5] S. M. Niu, Y. Liu, S. H. Wang, L. Lin, Y. S. Zhou, Y. F. Hu, Z. L. Wang, *Adv. Funct. Mater.* **2014**, *24*, 3332.
[6] S. W. Chen, C. Z. Gao, W. Tang, H. R. Zhu, Y. Han, Q. W. Jiang, T. Li, X. Cao, Z. L. Wang, *Nano Energy* **2015**, *14*, 217.
[7] J. Yang, J. Chen, Y. Yang, H. L. Zhang, W. Q. Yang, P. Bai, Y. J. Su, Z. L. Wang, *Adv. Energy Mater.* **2014**, *4*, 1.
[8] W. Tang, T. Jiang, F. R. Fan, A. F. Yu, C. Zhang, X. Cao, Z. L. Wang, *Adv. Funct. Mater.* **2015**, *25*, 3718.
[9] G. Zhu, P. Bai, J. Chen, Z. L. Wang, *Nano Energy* **2013**, *2*, 688.
[10] P. Bai, G. Zhu, Q. S. Jing, J. Yang, J. Chen, Y. J. Su, J. S. Ma, G. Zhang, Z. L. Wang, *Adv. Funct. Mater.* **2014**, *24*, 5807.
[11] Z. H. Lin, G. Cheng, S. M. Lee, K. C. Pradel, Z. L. Wang, *Adv. Mater.* **2014**, *26*, 4690.
[12] Y. N. Xie, S. H. Wang, S. M. Niu, L. Lin, Q. S. Jing, Y. J. Su, Z. Y. Wu, Z. L. Wang, *Nano Energy* **2014**, *6*, 129.
[13] F. Yi, L. Lin, S. M. Niu, J. Yang, W. Z. Wu, S. H. Wang, Q. L. Liao, Y. Zhang, Z. L. Wang, *Adv. Funct. Mater.* **2014**, *24*, 7488.
[14] G. Zhu, Y. J. Su, P. Bai, J. Chen, Q. S. Jing, W. Q. Yang, Z. L. Wang, *ACS Nano* **2014**, *8*, 6031.
[15] K. Q. Xia, Z. Y. Zhu, H. Z. Zhang, C. L. Du, Z. W. Xu, R. G. Wang, *Nano Energy* **2018**, *50*, 571.
[16] K. Q. Xia, Z. Y. Zhu, H. Z. Zhang, C. L. Du, Z. W. Xu, *Appl. Phys. A* **2018**, *124*, 520.
[17] Z. H. Lin, G. Cheng, Y. Yang, Y. S. Zhou, S. M. Lee, Z. L. Wang, *Adv. Funct. Mater.* **2014**, *24*, 2810.
[18] Q. Q. Shen, X. K. Xie, M. F. Peng, N. Sun, H. Y. Shao, H. H. Zheng, Z. Wen, X. H. Sun, *Adv. Funct. Mater.* **2018**, *28*, 1703420.
[19] J. Yang, J. Chen, Y. Liu, W. Q. Yang, Y. J. Su, Z. L. Wang, *ACS Nano* **2014**, *8*, 2649.
[20] J. Yang, J. Chen, Y. J. Su, Q. S. Jing, Z. L. Li, F. Yi, X. N. Wen, Z. N. Wang, Z. L. Wang, *Adv. Mater.* **2015**, *27*, 1316.
[21] S. H. Wang, L. Lin, Y. N. Xie, Q. S. Jing, S. M. Niu, Z. L. Wang, *Nano Lett.* **2013**, *13*, 2226.
[22] S. M. Niu, X. F. Wang, F. Yi, Y. S. Zhou, Z. L. Wang, *Nat. Commun.* **2015**, *6*, 8975.
[23] Y. F. Hu, J. Yang, S. M. Niu, W. Z. Wu, Z. L. Wang, *ACS Nano* **2014**, *8*, 7442.
[24] G. Cheng, Z. H. Lin, L. Lin, Z. L. Du, Z. L. Wang, *ACS Nano* **2013**, *7*, 7383.
[25] Y. F. Li, G. Cheng, Z. H. Lin, J. Yang, L. Lin, Z. L. Wang, *Nano Energy* **2015**, *11*, 323.
[26] G. Cheng, L. Zheng, Z. H. Lin, J. Yang, Z. L. Du, Z. L. Wang, *Adv. Energy Mater.* **2015**, *5*, 1.
[27] G. Cheng, Z. H. Lin, Z. L. Du, Z. L. Wang, *Adv. Funct. Mater.* **2014**, *24*, 2892.
[28] Y. L. Zi, J. Wang, S. H. Wang, S. M. Li, Z. Wen, H. Y. Guo, Z. L. Wang, *Nat. Commun.* **2016**, *7*, 10987.
[29] J. J. Yang, F. Yang, L. Zhao, W. Y. Shang, H. F. Qin, S. J. Wang, X. H. Jang, G. Cheng, Z. L. Du, *Nano Energy* **2018**, *46*, 220.

[30] G. Cheng, H. W. Zheng, F. Yang, L. Zhao, M. L. Zheng, J. J. Yang, H. F. Qin, Z. L. Du, Z. L. Wang, *Nano Energy* **2018**, *44*, 208.

[31] F. B. Xi, Y. K. Pang, W. Li, T. Jiang, L. M. Zhang, T. Guo, G. X. Liu, C. Zhang, Z. L. Wang, *Nano Energy* **2017**, *37*, 168.

[32] X. L. Cheng, L. M. Miao, Y. Song, Z. M. Su, H. T. Chen, X. X. Chen, J. X. Zhang, H. X. Zhang, *Nano Energy* **2017**, *38*, 438.

[33] W. Y. Shang, G. Q. Gu, F. Yang, L. Zhao, G. Cheng, Z. L. Du, Z. L. Wang, *ACS Nano* **2017**, *11*, 8796.

[34] Z. L. Li, J. Chen, J. Yang, Y. J. Su, X. Fan, Y. Wu, C. W. Yu, Z. L. Wang, *Energy Environ. Sci.* **2015**, *8*, 887.

[35] J. Chung, H. Yong, H. Moon, S. T. Choi, D. Bhatia, D. Choi, D. Kim, S. Lee, *Adv. Energy Mater.* **2018**, *8*, 1703024.

[36] Y. L. Zi, S. M. Niu, J. Wang, Z. Wen, W. Tang, Z. L. Wang, *Nat. Commun.* **2015**, *6*, 8376.

[37] S. Coe-Sullivan, W. K. Woo, J. S. Steckel, M. Bawendi, V. Bulović, *Org. Electron.* **2003**, *4*, 123.

[38] P. T. K. Chin, R. A. M. Hikmet, R. A. J. Janssen, *J. Appl. Phys.* **2008**, *104*, 013108.

[39] Y. X. Yang, Y. Zheng, W. R. Cao, A. Titov, J. Hyvonen, J. R. Manders, J. G. Xue, P. H. Holloway, L. Qian, *Nat. Photonics* **2015**, *9*, 259.